Solid Freeform Fabrication 2016: Proceedings of the 27th Annual International Solid Freeform Fabrication Symposium – An Additive Manufacturing Conference
Reviewed Paper

IN-SITU TiC PARTICLE REINFORCED 316L STAINLESS STEEL MATRIX NANOCOMPOSITES: POWDER PREPARATION BY MECHANICAL ALLOYING AND SELECTIVE LASER MELTING BEHAVIOUR

B. AlMangour[×]*, D. Grzesiak[†], J. M.Yang[×]

[×]Department of Materials Science and Engineering, University of California Los Angeles, Los Angeles, CA 90095, USA

[†]Department of Mechanical Engineering and Mechatronics, West Pomeranian University of Technology, Szczecin, Poland

*Corresponding author:

Email: balmangour@gmail.com

Abstract

In this study, mechanical alloying of 316L–Ti–graphite elemental powder mixture was performed to synthesize nanocomposite powder with 316L stainless steel matrix reinforced by in-situ formed TiC particles. Selective Laser Melting (SLM), an additive manufacturing process, of as-prepared TiC/316L composite powder was performed. It was found that the relative density, microstructure and mechanical properties of the SLM-processed nanocomposites were sensitive to the applied energy density. In general, the improvements in the mechanical properties are attributed to the combined effects of grain refinement and grain boundary strengthening. We believe that the alternative fabrication route presented in this study should significantly increase the use of nanocomposites.

Keywords: mechanical alloying; selective laser melting; porosity; hardness; wear

Introduction

316L stainless steel alloy is of great interest in the industry for their superior ductility and excellent corrosion resistance [1]. However, the applications of these alloys have been limited due to their poor strength and wear resistance both at room and high temperatures [2, 3]. To overcome this problem, 316L alloys may be strengthened by a uniform dispersion of very hard fine ceramic particles [4]. The majority of reinforcing powders are directly added to metal matrix (i.e. ex-situ composites). The interface between the reinforcing particles and metal matrix is often a potential source of weakness due to differences in their thermal expansion coefficients. When ceramic particulates are incorporated by an ex-situ process, a thin oxide layer is formed on the surface of the particulates. This oxide layer affects the bonding with the metal matrix and may cause a crack that may propagate from the interface [5-8].

To overcome such problems, several attempts have been made towards the development of in-situ MMCs in which the reinforcements are synthesized through a chemical reaction in the starting elemental materials [9]. In-situ formed ceramic reinforcements are thermodynamically stable in the matrix [10], leading to less degradation in elevated temperature applications. In particular, the reinforcement-matrix interface within in-situ MMCs are generally cleaner and more

compatible (i.e. free from gas absorption or oxidation) yielding stronger interfacial bonding and enhanced mechanical properties of the final products [11, 12].

Apart from powder preparation, the use of additive manufacturing (AM) to consolidate metal powders into three-dimensional shapes with complex geometries has attracted considerable interest in the recent years. Selective Laser Melting (SLM) is an AM process that builds parts layer-by-layer with a moving laser beam that selectively fuses and consolidates thin layers of loose powder [13-15]. In previous work [16], we have studied the influence of starting TiC particle size and volume content in the developed 316L nanocomposite. The composites were developed by ex-situ powder preparation method.

This study is aimed at the synthesis of in-situ TiC particles from pure Ti and pure C for reinforcement of 316L stainless steel. TiC particles can be formed by direct reaction between elemental Ti and graphite powder. Composite powders obtained after 35 h of milling were fabricated using SLM.

Experimental procedures

Feedstock powder, and SLM processes

The starting powder materials were: water-atomized 316L having an irregular shape and an average particle size of 44 µm (Fig. 1a), Ti possessing a polygonal structure and a mean particle size of 10 µm (Fig. 1b), and pure graphite with a mean particle size of 2-12 µm (Fig. 1c). A powder mixture containing 90 vol.% 316L, 8 vol.% Ti, and 2 vol.% graphite was mechanically alloyed under a vacuum atmosphere using a Pulverisette 6 planetary high-energy ball mill. The milling conditions and parameters used for powder preparation are highlighted in Table 1.

Specimens after 35 h of milling were used as a feedstock to be processed using the SLM parameters given in Table 2. Cylindrical specimens with dimensions of 8 mm x 10 mm were produced.

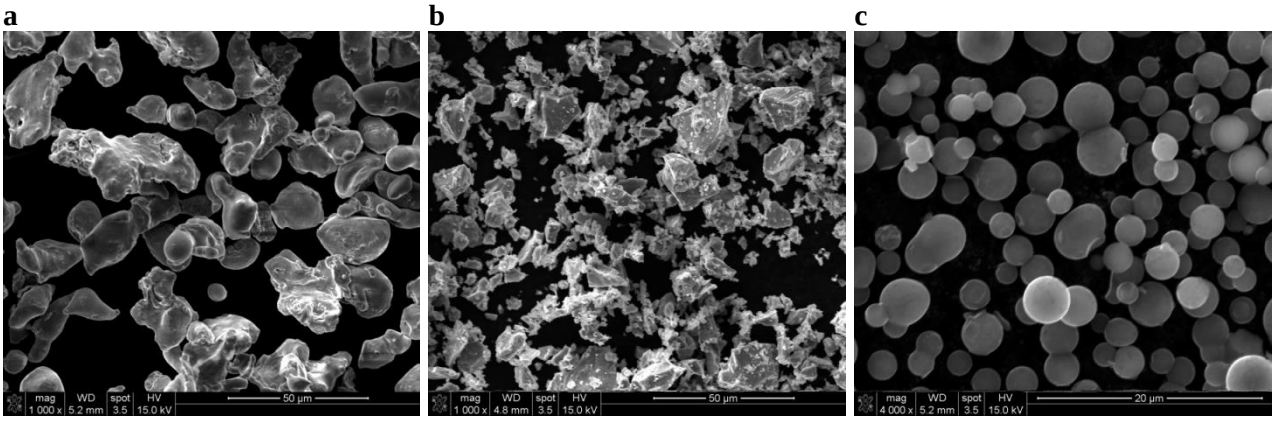

Figure 1: SEM micrograph of (a) 316L stainless steel powder; (b) Ti powder; (c) graphite powder.

Table 1: Milling conditions.

Atmosphere	Rotational speed	Balls	Ball/weight ratio	Vessel
vacuum	82 RPM	¼ stainless steel	9:1	4.8" OD x 10" Long

Table 2: SLM processing parameters.

Power for area volume	Atmosphere	Applied energy density (J/mm^3)	Layer thickness
100 W	Argon	67, 100, 200, 300	50 µm

Microstructural characterizations

Samples were mechanically grounded and polished with progressively finer grit papers using the standard metallographic techniques and etched in Marble's Reagent for 10s. The microstructures of the composite powder and the SLM-processed samples were observed using a Nova 230 Nano scanning electron microscope (SEM). The chemical compositions of the powder were determined with an EDAX energy-dispersive X-ray spectroscopy (EDX) system. The samples' density was measured using the conventional Archimedes' principle.

Mechanical testing

Vickers indentations was performed (Leco, LM800AT) at a load of 200 g at 15 random locations. Dry sliding wear tests were performed on the SLM-processed samples using a T50 ball-on-disk tribometer at room temperature as per the ASTM G99 standard. A 3-mm-diameter 52100 bearing steel ball was used as the counterface material. A load of 3 N was used during the tests. The friction unit was rotated at 840 rpm for 20 min; the rotation radius was 2 mm. The volume of material lost was measured using a ST400 white-light profilometer. The profilometer had a vertical resolution and accuracy of 8 and 80 nm, respectively, and a lateral resolution of 2 µm. The cross-sectional area of the wear track was multiplied by the circumference of the wear track to get the total volume of material removed. This volume was then divided by the load applied and the total distance traveled during the test to calculate the wear rate of the material (mm^3/N m). When the same test parameters are used for a number of samples, the wear rate can be used as a quantitative metric for comparing the wear resistances.

Results

Powder characterizations

Figure 2 shows the evolution of the morphologies of milled powders with the applied milling times. These micrographs show that the microstructural characteristics of milled powders (e.g., particle shape, particle size and its distribution, powder dispersion state) were significantly influenced by the milling times applied. The soft 316L stainless steel particles were flattened in the early stage of milling and turned into flake-like particles after longer hours of milling. The Ti particles were able to undergo plastic deformation but the brittle C particles did not undergo plastic deformation or cold welding in the early stage of milling. The impact forces on the

particles imposed by the grinding medium caused severe plastic deformation of 316L particles and cold-welding to form larger particles. Further milling caused the particles to be work-hardened and the fracture mechanism to prevail over the cold welding process.

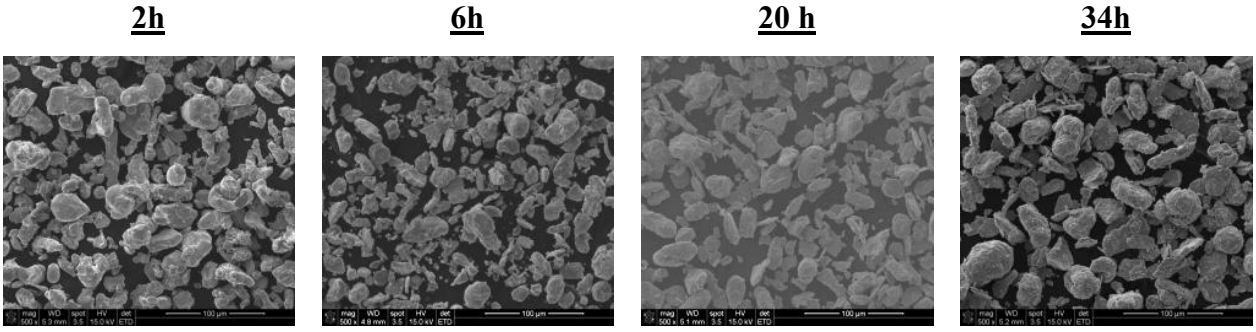

Figure 2: SEM micrograph of milled feedstock powder at different milling times.

To further study the chemical composition of the milled powders, EDX characterization in selected areas of SEM images, was performed as indicated in Fig. 3. For a relatively short milling time of 2 h, the weight content of Ti and C detected on the particle surface was quite low. This may have been due to low dissolution of 316L atoms in the Ti lattice in the initial stages of milling. The elemental concentration of Ti and C on the particle surface increased abruptly when the milling time increased. From this observation, we can conclude that a large number of regions where C atoms are dissolved in Ti lattice start to appear on the surfaces of milled powders, creating primary TiC solid solution zones. The EDX results showed that for milling up to 34 h however the weight fraction of 316L on the surface of milled particles decreased. This can be explained by considering that more 316L atoms penetrated deep from the surface into the interior regions of Ti particles and dissolved in the whole Ti volume, forming a TiC solid solution. This could also be due to the fracture of 316L matrix powder particles causing fresh surfaces to be continuously created.

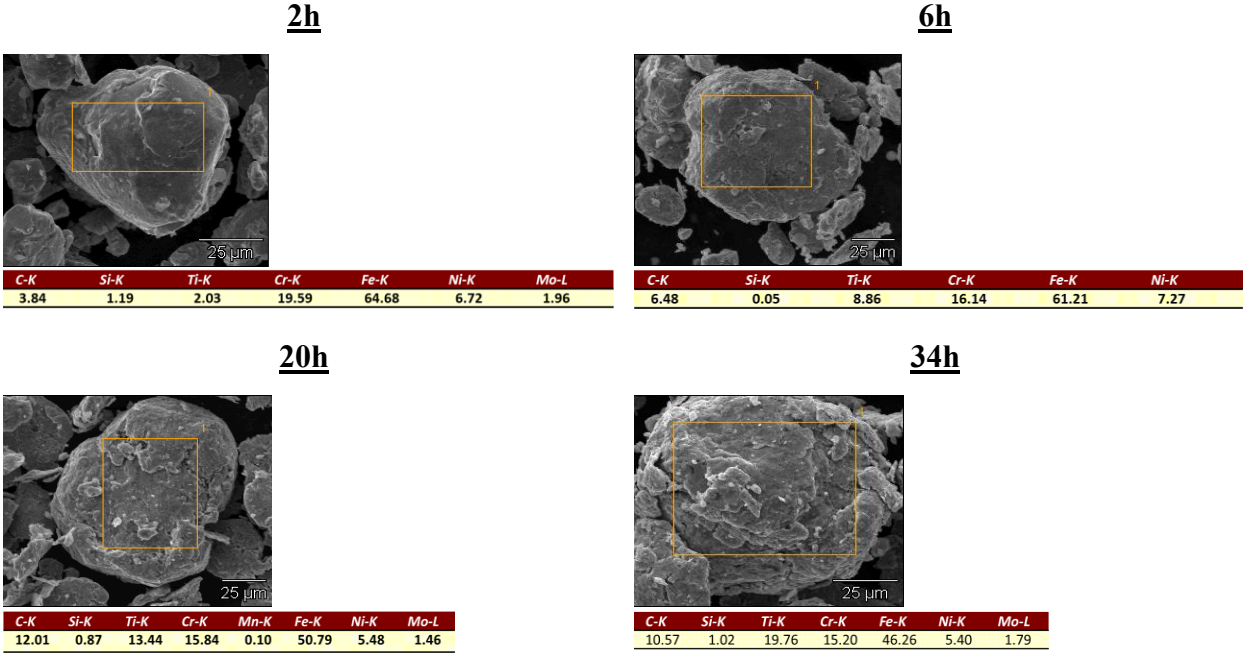

Figure 3: EDX analysis of milled feedstock powder at different milling times.

SLM-processed composites characterizations

Figure 4 shows the low-magnification images for the etched composites samples using applied energy density of 67 (Fig. 4a) and 100 J/mm^3 (Fig. 4b). Table 3 illustrates the density of the fabricated nanocomposite as a function of milling time. Clearly, the applied energy density affects the densification of the SLM-processed parts. On increasing the applied energy density from 67 to 100 J/mm^3, the densification level increased to 98.62%, which was further dropped sharply to 88.81% at a higher energy density of 300 J/mm^3. The corresponding microstructure at low energy densities (Fig. 4) showed that a number of balls were formed. Further details of SLM densification will be given in the discussion section.

a **b**

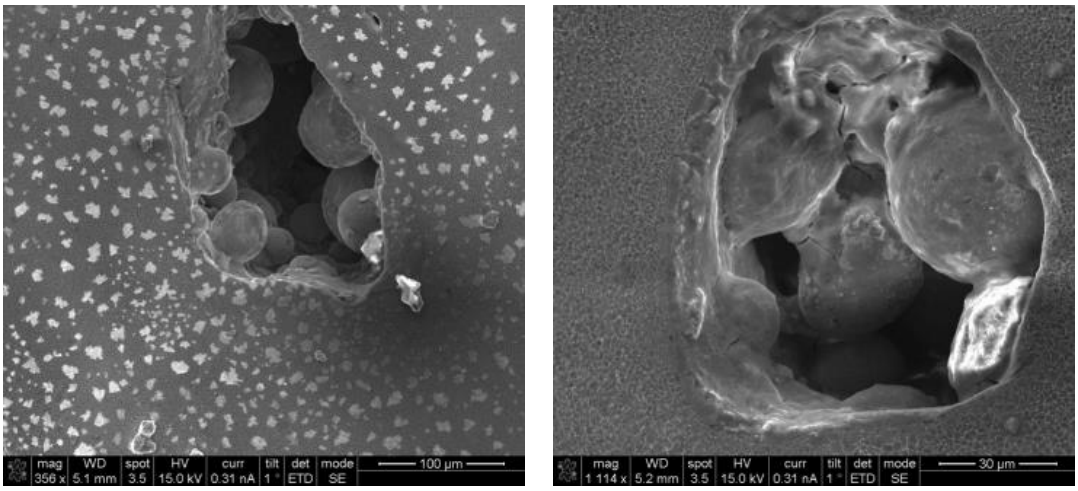

Figure 4: Etched microstructure of the SLM-fabricated composites using different applied energy density (E): (a) 67; (b) 100.

Table 3: Variation of relative density as a function of the applied energy density.

SLM applied energy density (J/mm^3)	**67**	**100**	**200**	**300**
Relative density (%)	95.52	98.62	89.55	88.81

Figure 5 shows the influence of the applied laser energy density on the characteristics microstructures in the SLM-processed composites. It was seen that grains are slightly of different sizes, may be due to the varying thermal heat fluxes during every scanning tracks. Nevertheless, a careful comparison of the microscopic features of these images revealed some distinct variations with the applied laser energy density. With increasing the energy density, the grains tend to coarsen as a result of the lower scanning speed that favor slower solidification rate.

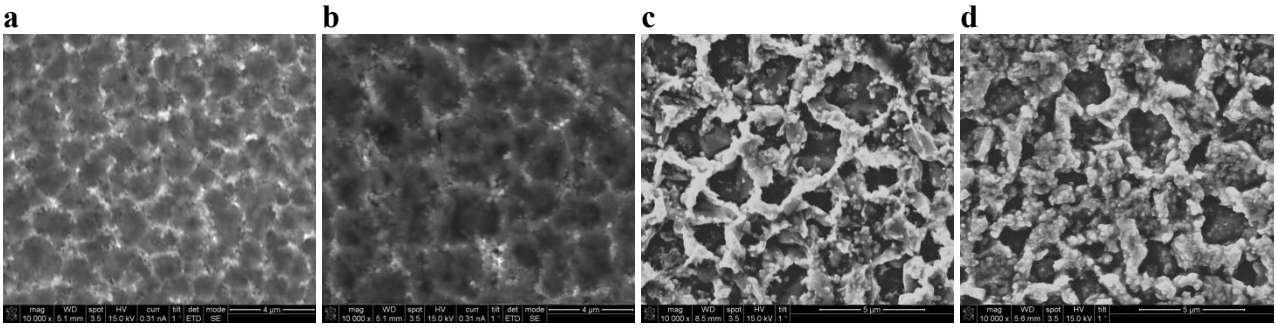

Figure 5: Etched microstructure of the SLM-fabricated composites using different applied energy density (E): (a) 67; (b) 100; (c) 200; (d) 300.

Mechanical behavior

Table 4 demonstrates the effect of the applied energy density of the 316L nanocomposites on the average microhardness and wear rate. The hardness were increased at 100 J/mm^3 and then dropped at the applied energy densities of 200-300 J/mm^3. The drop in hardness after applying higher energy density is a result of grain growth. Interestingly, the hardness exhibited similar trend as the relative density with respect to the applied energy density. This suggests that the applied energy density played an important role in influencing the relative density, microhardness and wear performance of the nanocomposite.

Table 4: Variation of microhardness and wear rate as a function of the applied energy density.

SLM applied energy density (J/mm^3)	**67**	**100**	**200**	**300**
Microhardness ($HV_{0.2}$)	379.38±26.46	385.94±36.46	341.62±56.62	370.83±51.73
Wear rate (mm^3/Nm)	2.271	2.061	1.405	1.596

Discussion

It was deduced that during laser processing, there is a strong likelihood of occurrence of the "balling phenomena" and unmelted particles (Fig. 4). This is the result of laser instability and insufficient applied energy density respectively [17]. The carbon content, used in this study, plays a critical role in determining processability of SLM. Indeed, the high carbon content also has adverse effect on SLM produced steel, since they portray a limited densification response. Wright et al. [18], found out that with increase in carbon contents, there is an increase in the thickness of the carbon layer accumulated on the melt surface. Just like the oxide layer, the carbon layer has a critical influence mostly on diminishing wettability and causing the melt to spheroidise rather than flow across the underlying surface. In addition to this, the brittleness of SLM manufactured high carbon content steel is increased by the formation of complex interfacial carbides at grain boundaries [19]. Childs et al. [20] concluded that the dissolution of carbides is favored by increasing the heat flow in the treated powder. On the same breath, increasing heat flow homogenizes distribution of alloying elements. Thus, the optimization of laser parameters is necessary. Due to this reason, high volumetric energy density for both elemental homogeneity and powder consolidation is achieved [15, 21, 22].

During the laser melting process, the metal powder absorbs the laser energy, raises its temperature, melt, and then solidifies when laser moves away, the whole process is less than one second. The heat also transfers away from the melt zone quickly. This causes the melt to cool down rapidly leading to short arrangement time and consequently porosity. In addition, because of the high cooling rate, the gas adsorbed on the surface of the powder, as well generated because of the reaction during the laser melting, have no time to escape from the molten pool and hence porosity was formed.

When free interfaces exist in the system (e.g. liquid-liquid, liquid-gas interfaces) the temperature and compositional gradient will impose a surface tension gradient along the interface, which exerts a shear stress on the fluid. This induces a flow toward regions with higher values of γ termed Marangoni convection [23]. It is observed that during scanning "balling" has occurred. This is caused by surface tension driven by Marangoni convection (i.e. melting instability). Because of the strongly concentrated energy source, a large temperature gradient is often induced on the surface. If the surface tension γ depends on temperature, then the temperature gradient induces a surface flow that can have a considerable influence on the melting pattern. If the surface tension increases with temperature ($d\gamma/ dT > 0$), the liquid moves toward the energy beam on the surface, inducing narrower and deeper pool. However, if the surface tension decreases with temperature ($d\gamma/ dT < 0$), the surface flow moves away from the energy beam, leading to a wider and shallower pool.

Conclusions

In-situ TiC particle reinforced 316L stainless steel powder has been successfully used in the SLM process. The effects of SLM applied energy density on the microstructure and mechanical properties were studied. The SLM processed parts show a uniform fine equiaxed microstructure. Further optimizations of the processing parameters are necessary for future work. We believe that in-situ MMCs fabricated by AM could be used to produce cheaper components that fulfill the increasing demand for high performance with their superior properties.

Acknowledgment

One of the authors, Bandar AlMangour, would like to extend his appreciation to the Saudi Basic Industries Corporation, which generously awarded financial support to him.

References

[1] AL-Mangour B. Powder Metallurgy of Stainless Steel: State-of-the Art, Challenges, and Development. Stainless Steel: Microstructure, Mechanical Properties and Methods of Application: Nova Science Publishers; 2015. p. pp. 37-80.
[2] Krishna DSR, Sun Y. Effect of thermal oxidation conditions on tribological behaviour of titanium films on 316L stainless steel. Surface and Coatings Technology 2005;198:447-53.
[3] Majumdar JD, Kumar A, Li L. Direct laser cladding of SiC dispersed AISI 316L stainless steel. Tribology International 2009;42:750-3.
[4] Abenojar J, Velasco F, Torralba J, Bas J, Calero J, Marce R. Reinforcing 316L stainless steel with intermetallic and carbide particles. Materials Science and Engineering: A 2002;335:1-5.
[5] Froyen L. In-situ processing of metal matrix composites. End of the wetting problems? Transactions of the JWRI(Japan) 2000;30:391-400.
[6] Tee K, Lü L, Lai M. Improvement in mechanical properties of in-situ Al–TiB 2 composite by incorporation of carbon. Materials Science and Engineering: A 2003;339:227-31.

[7] Erich DL. Metal-matrix composites: problems, applications, and potential in the P/M industry. International journal of powder metallurgy (1986) 1987;23:45-54.
[8] Ibrahim I, Mohamed F, Lavernia E. Particulate reinforced metal matrix composites—a review. Journal of materials science 1991;26:1137-56.
[9] Matin M, Lu L, Gupta M. Investigation of the reactions between boron and titanium compounds with magnesium. Scripta Materialia 2001;45:479-86.
[10] Tjong SC. Novel Nanoparticle-Reinforced Metal Matrix Composites with Enhanced Mechanical Properties. Advanced engineering materials 2007;9:639-52.
[11] Krasnowski M, Kulik T. Nanocrystalline FeAl–TiN composites obtained by hot-pressing consolidation of reactively milled powders. Scripta materialia 2007;57:553-6.
[12] Tjong SC, Ma Z. Microstructural and mechanical characteristics of in situ metal matrix composites. Materials Science and Engineering: R: Reports 2000;29:49-113.
[13] Rombouts M, Kruth J-P, Froyen L, Mercelis P. Fundamentals of selective laser melting of alloyed steel powders. CIRP Annals-Manufacturing Technology 2006;55:187-92.
[14] Kruth J-P, Levy G, Klocke F, Childs T. Consolidation phenomena in laser and powder-bed based layered manufacturing. CIRP Annals-Manufacturing Technology 2007;56:730-59.
[15] Yadroitsev I, Shishkovsky I, Bertrand P, Smurov I. Manufacturing of fine-structured 3D porous filter elements by selective laser melting. Applied Surface Science 2009;255:5523-7.
[16] AlMangour B, Grzesiak D, Yang J-M. Selective laser melting of TiC reinforced 316L stainless steel matrix nanocomposites: Influence of starting TiC particle size and volume content. Materials & Design 2016.
[17] AlMangour B, Grzesiak D, Yang J-M. Rapid fabrication of bulk-form TiB_2/316L stainless steel nanocomposites with novel reinforcement architecture and improved performance by selective laser melting. Journal of Alloys and Compounds 2016;680:480-93.
[18] Wright CS, Youseffi M, Akhtar S, Childs T, Hauser C, Fox P. Selective laser melting of prealloyed high alloy steel powder beds. Materials science forum: Trans Tech Publ; 2006. p. 516-23.
[19] Childs T, Hauser C, Badrossamay M. Selective laser sintering (melting) of stainless and tool steel powders: experiments and modelling. Proceedings of the Institution of Mechanical Engineers, Part B: Journal of Engineering Manufacture 2005;219:339-57.
[20] Childs T, Hauser C, Badrossamay M. Mapping and modelling single scan track formation in direct metal selective laser melting. CIRP Annals-Manufacturing Technology 2004;53:191-4.
[21] Tsopanos S, Mines R, McKown S, Shen Y, Cantwell W, Brooks W, et al. The influence of processing parameters on the mechanical properties of selectively laser melted stainless steel microlattice structures. Journal of Manufacturing Science and Engineering 2010;132:041011.
[22] Gusarov A, Yadroitsev I, Bertrand P, Smurov I. Heat transfer modelling and stability analysis of selective laser melting. Applied Surface Science 2007;254:975-9.
[23] Davis SH. Theory of solidification: Cambridge University Press; 2001.